https://doi.org/10.5194/egusphere-2025-6271
Preprint. Discussion started: 12 January 2026

Light Absorption Properties and Composition of Brown carbon in North China Plain: Implication for an Enhancing Role of Nitrogenous Organic Compounds

Can Wu [1,2], Huijun Zhang[1], Kehan Sun [1], Rongjie Li[1], Ziting Yan[1], Yubao Chen[1], Zheng Li[1], Binyu Xiao[1], Yanqin Ren[3], Gehui Wang*[1,2]

[1]Key Lab of Geographic Information Science of the Ministry of Education, School of Geographic Sciences, East China Normal University, Shanghai 210062, China
[2] Institute of Eco-Chongming, 3663 North Zhongshan Road, Shanghai 200062, China
[3]State Key Laboratory of Environmental Criteria and Risk Assessment, Chinese Research Academy of Environmental Sciences, Beijing 100012, China

*Corresponding author.
Mailing address: School of Geographic Sciences, East China Normal University, Shanghai 210062, China
E-mail address: ghwang@geo.ecnu.edu.cn

https://doi.org/10.5194/egusphere-2025-6271
Preprint. Discussion started: 12 January 2026

Abstract: Brown carbon (BrC), an efficiently light-absorbing carbonaceous aerosol, exerts significant impacts on the global energy budget and regional climate, attracting growing scientific attention. To advance understanding of the spatial variability of atmospheric BrC and its dominant formation pathways in the North China Plain (NCP), light absorption properties, chemical composition and formation process of the water-soluble BrC in 2023 winter were investigated by conducting simultaneous measurements at five sites across the NCP, namely, Beijing, Tianjin, Luancheng (rural site), Handan and Jinan. Our results showed that the average light absorption coefficient at 365 nm (abs_{365}) in Luancheng was approximately 1.1–3.5 times higher than those in urban ones; While mass absorption efficiency displayed a distinctly different spatial pattern, with the strongest light-absorptivity (1.40±0.02 m^2 g^{-1}) recorded in Jinan. Notably, average abs_{365} in four urban sites exhibited a decline of ~45% from 2018 to 2023 compared to those previous observations. Furthermore, the light-absorptivity of BrC was enhanced from clean to haze period at the most sampling sites along with the increasing N:C ratio, indicating that nitrogenous organic compounds (NOCs) were the important BrC chromophores in the NCP. Additionally, more than 50% of NOCs were confirmed to be secondarily formed; and the ammonia-driven aqueous reactions were identified as the predominant pathway governing the secondary formation of these NOCs. These results elucidate the substantial contribution of NOCs to atmospheric BrC in the NCP, and further confirm the importance of ammonia emission for alleviating haze and BrC pollution in this region.

Keywords: Brown carbon; Nitrogenous organic compounds; Spatiotemporal

https://doi.org/10.5194/egusphere-2025-6271
Preprint. Discussion started: 12 January 2026

characteristics; Biomass burning; Secondary formation

1. Introduction

Light-absorbing organic aerosol, optically defined as brown carbon (BrC), is prevalent in the troposphere and efficiently absorbs solar radiation, thereby perturbing the global energy budget and influencing regional climate (Liu et al., 2020; Laskin et al., 2015; Samset et al., 2018). Recent modeling studies demonstrates that BrC is responsible for >20% of the direct radiative effect (DRE) caused by carbonaceous aerosols (Zeng et al., 2020; Feng et al., 2013; Zhang et al., 2017; Liu et al., 2015a); Most significantly, BrC even dominates the DRE in certain regions of the Earth, e.g., in the remote tropical upper troposphere (Zhang et al., 2020). However, these reported BrC DRE have large uncertainty, partly stemming from the poor understanding of optical properties and atmospheric evolution of BrC. Unlike black carbon (BC), BrC is characterized by a pronounced dependence of light-absorption on wavelength, with absorbance increasing steeply near UV wavelengths (Andreae and Gelencsér, 2006); Consequently, abundant BrC can also reduce the amount of ultraviolet sunlight reaching surface, subsequently altering tropospheric photochemistry. Indeed, growing evidence reveal a nonnegligible reduction in photolysis rates of the ozone and radicals with enhanced BrC load (Hammer et al., 2016; Gligorovski et al., 2015; Jo et al., 2016; He and Carmichael, 1999). Beyond the climatic and atmospheric effects, multiple BrC chromophores (e.g, polycyclic aromatic and nitro-heterocyclic compounds) also pose adverse health effects because of their strong oxidative potential (Fang et al., 2019; Daellenbach et al., 2020).

Diverse sources of atmospheric BrC have been identified, including the various

https://doi.org/10.5194/egusphere-2025-6271
Preprint. Discussion started: 12 January 2026

primary emissions and complex secondary formation. Primary BrC is known to be directly emitted from the incomplete combustion of biomass and other fuels (Washenfelder et al., 2015; Lack et al., 2012; Chen et al., 2017; Yan et al., 2017), of which optical properties are inherently related to combustion conditions and fuel types (Ni et al., 2021; Xie et al., 2017; Stockwell et al., 2015). And field measurements and laboratory studies indicated that the aromatics, conjugated systems, and highly functionalized species with high light-absorptivity can be secondarily formed via $OH\cdot/NO_3\cdot/O_3$ photooxidation of various precursors (Hems and Abbatt, 2018; Jiang et al., 2019; Finewax et al., 2018), or reactions initiated by ammonia/amines with atmospherically relevant carbonyls (Updyke et al., 2012; Powelson et al., 2014; Grace et al., 2020). These processes would generate abundant N-containing compounds (NOCs), which have been recognized as significant components of BrC (Lin et al., 2015; Yang et al., 2022; Wang et al., 2025a). Notably, the latest modeling study suggested that the NOCs dominate the global organic aerosol absorption, accounting for 18% of global DRE induced by carbonaceous aerosols (Li et al., 2025); And these absorptive NOCs are probably responsible for an enhanced light absorption of BrC in the upper boundary layer, as a result of their efficient formation in the lifting air masses (Wu et al., 2024a; Wu et al., 2024b). Moreover, the further aging processes would chemically modify the BrC composition, subsequently leading to either an increase (photodarkening) or decrease (photobleaching) in light-absorptivity of BrC chromophores (Wong et al., 2017; Jiang et al., 2022; Hems et al., 2021). These dynamic natures of BrC drive pronounced spatiotemporal heterogeneity in its chemical components and optical

https://doi.org/10.5194/egusphere-2025-6271
Preprint. Discussion started: 12 January 2026

properties, propagating significant uncertainties in climate models that limit the reliable projection and mitigation of the climate effects caused by diverse BrC.

Over the past decade, the stringent emission control measures have been implemented in the North China Plain (NCP), for which BrC level was expected to drastically decrease due to the significant contribution of primary emission to atmospheric BrC (Chen et al., 2024b; Zheng et al., 2018); Nevertheless, high loads of strongly light-absorbing BrC were still detected frequently in this region (Wang et al., 2025c; Chen et al., 2024a; Gong et al., 2023; Sun et al., 2026). Therefore, the sources and formation mechanism remain elusive in the NCP. Moreover, the atmospheric environment in this region also undergone significant changes, characterized particularly by the increase in oxidation capacity and NH_3 levels (Fu et al., 2017; Li et al., 2019). Our recent studies demonstrate that such an ammonia-rich environment plays a key role in enhancing BrC absorption, primarily by reducing aerosol acidity and facilitating the formation of light-absorbing NOCs (Liu et al., 2023; Zhang et al., 2024); These findings imply that the primary drivers of BrC formation may have changed relative to those in the past. Motivated by this, atmospheric BrC in the NCP were collected during the 2023 winter and analyzed for the characteristics of BrC. We investigated the spatial difference of chemical composition and light-absorption of BrC, and discussed the role of NOCs in the BrC light absorption and their formation pathways.

2. Materials and Methods

2.1 Sampling

https://doi.org/10.5194/egusphere-2025-6271
Preprint. Discussion started: 12 January 2026

The multi-site observations were synchronously conducted on the North China Plain from 15 November to 31 December 2023 (Figure S1). Four of the sampling sites are located in urban areas, namely Beijing (BJ), Tianjin (TJ), Handan (HD) and Jinan (JN), which are surrounded by the traffic arteries and dense residential and commercial buildings. And the remaining one, adjacent to Luancheng (LC), serves as a rural station free from significant industrial influences. At each site, the $PM_{2.5}$ samples with a 12-hr interval were collected onto prebaked (at 450°C for 6 hrs) quartz filters using high- ($1.13\ m^3\ min^{-1}$) or medium-volume ($100\ L\ min^{-1}$) air samplers; All the samplers located on the rooftops approximately 15–20 m above ground level. After sampling, the filter samples were wrapped in prebaked aluminum foils and stored in a freezer (at -18°C) prior to analysis.

Hourly concentrations of $PM_{2.5}$ and associated pollutants (e.g., NO_2, O_3, CO) at the sampling sites were obtained from the National Urban Air Quality Real-time Release Platform of China (https://air.cnemc.cn:18007/, last access: 6 April 2025), of which monitoring sites are adjacent to ours with a distance of < 10 km. The meteorological data including ambient temperature (T) and relative humidity (RH) were downloaded from National Climatic Data Center (https://www.ncei.noaa.gov/, last access: 6 April 2025).

2.2 Chemical analysis

A piece of each filter was extracted with 40 ml the ultrapure Milli-Q water (18.2 MΩ) under ultrasonication for 30 min. A part of the extract was used for the detection of water-soluble ions (SO_4^{2-}, NO_3^-, Cl^-, Na^+, NH_4^+, K^+, Mg^{2+} and Ca^{2+}) by using an ion

https://doi.org/10.5194/egusphere-2025-6271
Preprint. Discussion started: 12 January 2026

chromatography; The remaining part was detected for the water-soluble organic carbon (WSOC) and water-soluble total nitrogen (WSTN) via a total organic carbon (TOC) analyzer (Model TOC-L CPH, Shimadzu, Japan). A DRI-model 2001 thermal–optical carbon analyzer following the IMPROVE-A protocol was applied here to measure organic carbon (OC) and element carbon (EC) of $PM_{2.5}$.

The molecular compositions in $PM_{2.5}$ samples, including nitro-aromatic compounds (NACs, Table S1), PAHs and others organic tracers, were extracted with a mixture of dichloromethane and methanol (2: 1, v/v); Subsequently, the extracts were derivatized via derivatization reagent (a mixture of 50 μl of N,O-bis-(trimethylsilyl)trifluoroacetamide (BSTFA) and 1 % trimethylsilyl chloride and 10 μl of pyridine) prior to GC/MS analyses. More details of the extraction, derivatization and the GC/MS analyses can refer to elsewhere (Wang et al., 2006; Wu et al., 2025).

Additionally, the Aerodyne high-resolution time-of-flight aerosol mass spectrometer (HR-AMS) was applied here to characterize the imidazole-related fragments (e.g., $C_3H_3N_2^+$ and $C_3H_4N_2^+$) in a typical humid haze event (12 to 31 December of 2023, Figure S2), following the method reported by Ge et al. (2024). A part of the $PM_{2.5}$ filter was extracted following the procedure similar to that of other water-soluble components; then the extracts were atomized using argon as the carrier gas, dehydrated by a diffusion drier, and ultimately quantified by HR-AMS. Each sample was continuously monitored by HR-AMS for >10 min to obtain stable signal, and above procedure was also applied to the blank samples to account for any potential contamination or background signals. Adeep post-processing was conducted for the V-mode data in this study using the Igor-

https://doi.org/10.5194/egusphere-2025-6271
Preprint. Discussion started: 12 January 2026

based Aerosol Mass Spectrometer Analysis Toolkit. The mass concentration of imidazole-related fragments was calculated as the follow:

$$C_{IMs}=F_{IMs}\times WSOM \quad (1)$$

Where C_{IMs} denotes to the concentration of the imidazole-related fragments. F_{IMs} is mass contribution of the imidazole-related fragments to the total fragments measured by HR-AMS; WSOM refers to atmospheric concentration of water-soluble organic matter (μg m^{-3})

2.3 Optical Absorption of BrC

The light-absorbing chromophores (i.e., BrC) were also extracted with 10 ml ultrapure Milli-Q water, following the procedure for water-soluble ions; A UV−vis spectrometer was applied here to record the absorption spectra of all the extracts, which were finally converted into absorption coefficient (abs_λ, M/m) at a given wavelength (λ) using the following equation:

$$abs_\lambda=(A_\lambda-A_{700})\frac{v_L}{v_a\times l}\times\ln(10) \quad (2)$$

Where A_λ is the absorbance at wavelength λ (nm), V_L and Va refer to the volume of the extractant and air through corresponding to filter punches, respectively. The optical path length is 1 cm (i.e, *l*). From abs_λ, the mass absorption coefficient (MAE_λ, m^2/g) can be characterized as:

$$MAE_\lambda=\frac{abs_\lambda}{C} \quad (3)$$

Where C is the mass concentration of water-soluble organic carbon.

2.4 Random forest analysis for water-soluble organic nitrogen

Random forest (RF), as a powerful tool for regression and prediction (Hu et al., 2017; Vu et al., 2019), was employed here to elucidate the relationships between secondary

https://doi.org/10.5194/egusphere-2025-6271
Preprint. Discussion started: 12 January 2026

WSON (WSONsec) and potential factors (NH_4^+, NO_2, O_3, ALWC, pH and meteorological factors), while determining the importance of each factor to WSONsec along with a SHAP analysis. In the RF model design, 70% of the dataset including all the samples from the five monitoring sites was randomly divided into a training subset to construct the RF model, and the remaining 30% (i.e., test set) was used to assess the model performance. Following systematic hyperparameter optimization, the decision tree (n_{tree}) was set to 300 to balance model performance and computational efficiency; and number of variables split at each node (n_{mtry}) was limited to 12 to avoid overfitting. Additionally, a 10-fold cross-validation strategy was adopted here to optimize model parameters and estimate model performance. The RF model was constructed using the "randomForest" R package, of which performance was evaluated by coefficient of determination (R^2), mean square error (MSE) or root-mean-square error (RMSE) and mean absolute error (MAE). As summarized in Table S2, the simulated WSONsec corrected strongly with observed ones, and the error metric remained at low levels; Thess indicated that the model could reconstruct commendably the variations of WSONsec in this study.

2.5 Theoretical estimation of particulate fraction of NACs (Fp)

Since gas-phase nitro-aromatic compounds (NACs) were not detected in this study, the particulate-phase fraction (F_p) of NACs was calculated based on absorption equilibrium theory (Pankow et al., 2001; Zuend and Seinfeld, 2012), and the specific calculation method referred to that reported by Chen et al. (2025). As shown in the following equations:

$$Fp=\frac{C_p}{C_p+C_g}=\frac{K_p\times PM}{1+K_p\times PM} \quad (4)$$

$$K_p=\frac{C_p}{C_g\times PM}=\frac{760\times f\times R\times T}{10^6\times P_V\times M\times \xi} \quad (5)$$

Herein, C_g and C_p are the mass concentrations of the organic molecule in gas and

https://doi.org/10.5194/egusphere-2025-6271
Preprint. Discussion started: 12 January 2026

particle phase, respectively. Kp refers to gas–particle partitioning coefficient, and is determine by many factors in Eq. 5. Specifically, Pv is the saturation pressure (Pa), which is 0.00378 torr for 4-nitrophenol (at 298 K); ξ is the activity coefficient of the species, adopting from the values reported by Wang et al. (2019); *f* is s the fraction of organic matter in the particle phase; M refers to the molecular weight of NAC species (g mol^{-1}); Additionally, R is the gas constant (8.314 J (mol K) $^{-1}$), T is the temperature (K), *f* denotes the fraction of organic matter in particle, and PM is the mass concentration of $PM_{2.5}$.

3. Result and discussion

3.1 Spatial variation of $PM_{2.5}$ Chemical Composition

As shown in Table 1 and Figure S2, the $PM_{2.5}$ concentration across the North China Plain (NCP) exhibited significant spatial heterogeneity, ranging from 4.0 to 223.7 μg m^{-3}. Specifically, the highest average $PM_{2.5}$ load was recorded in JN (94.1±37.8 μg m^{-3}), partially attributed to unfavorable topographic conditions and intensive anthropogenic emissions; The average $PM_{2.5}$ level at remaining sampling sites decreased gradually from south to north. Notably, the $PM_{2.5}$ concentration in Beijing during the campaign was only a quarter of that recorded a decade ago (158 μg m^{-3}), indicating a notable air quality improvement in BJ over recent years. Even so, multi-day haze episodes ($PM_{2.5}$>75 μg m^{-3}) still occurred frequently in BJ (Figure S1), of which hourly peak concentration even reached up to 203 μg m^{-3}, about 3-flod of National Air Quality Standard grade-II (75 μg m^{-3}). Additionally, these events were also observed simultaneously at other sites, suggesting that regional $PM_{2.5}$ pollution remains

https://doi.org/10.5194/egusphere-2025-6271
Preprint. Discussion started: 12 January 2026

a persistent challenge during winter across the NCP, particularly in its southern region.

The spatiotemporal differences in chemical compositions, sources of organic matter (OM) in $PM_{2.5}$ among sampling sites are illustrated in Figure 1. As the major component of $PM_{2.5}$, water soluble ions (WSIs) accounted for approximately 30%-53% of $PM_{2.5}$; Similar to the spatial pattern of $PM_{2.5}$, WSIs also exhibited high loads in JN (40.4±23.2 μg m^{-3}) and HD (44.1±34.3 μg m^{-3}), which were ~1.2-4 fold of those measured in other sites. From Figure 1, nitrate was the most abundant ion across the NCP, accounting for 14%-27% of $PM_{2.5}$, followed by sulfate (5%-9%) and ammonium (4%-11%), respectively. Compared to those in urban sites, relative abundance of SNA (SO_4^{2-}, NO_3^- and NH_4^+) in rural site (LC) moderately enhanced by 10%-23%, indicating a significant influence of secondary aerosol formation in the rural area. Furthermore, a relatively high concentration of chloride was detected among the sampling sites, even with a molarity being >1.5-fold of that of sulfate (Figure S3a). A strong correlation between chloride and levoglucosan+BkF across the sampling sites (R^2=0.97) implied that combustion emissions were the primary source for the abundant chloride in the NCP (Figure S3b). These abundant chlorides could promote heterogeneous formation of sulfate as evidenced by a robust relationship chloride and SOR ($SO_4^{2-}/(SO_4^{2-}+SO_2)$) (Figure S3c). This finding was consistent with the results of our laboratory experiments (Wang et al., 2025b; Wang et al., 2016), which demonstrated that the abundant chloride could significantly enhance the uptake of NO_2 by interfacial electrostatic attraction, subsequently accelerating sulfate formation.

The average concentration of OM ranged from 7.9±5.7 μg m^{-3} to 18.7±10.7 μg m^{-3},

https://doi.org/10.5194/egusphere-2025-6271
Preprint. Discussion started: 12 January 2026

accounting for 17%-25% of $PM_{2.5}$. Although OM was a predominant species in $PM_{2.5}$ at most sites, its spatial distribution differed slightly from that of $PM_{2.5}$, with high loads in LC (18.5±11μg m^{-3}) and HD (18.7±10.7 μg m^{-3}). To determine the sources of the abundant OM, a PMF was applied here and identified three types OM sources (Figure S4, Text S1). From Figure 1, a significant fraction of OM (40%-55%) at urban sites was associated with secondary formation, comparable to that in northern regions of China (50%) (Chen et al., 2024b); In contrast, combustion-derived primary OM accounted for less than 40% of the total OM; This finding was consistent with the filed observations which demonstrated a widespread decline in primary OM in NCP during 2013-2020 due to the significant reduction in residential fuel burning (Chen et al., 2024b). Notably, about 55% of OM at rural site was derived from combustion, reflecting an urban-rural variation in sources.

3.2 Spatial variability in optical properties of BrC

Figure 2a displays the average absorption spectra of WSOC across the sampling sites, which exhibits the marked feature of BrC with the reduced light absorption from the ultraviolet to the visible ranges. As illustrated in Table 1 and Figure 2, the light absorption coefficient at 365 nm (abs_{365}) displayed a spatial pattern similar to that of organic matter (OM) across the five sampling sites; Specifically, the highest average abs_{365} was observed at LC site, with average of (8.0±4.7 Mm^{-1}), followed by HD (7.9 ±5.0 Mm^{-1}), JN (6.9±3.0 Mm^{-1}), TJ (5.7±3.8 Mm^{-1}) and BJ (2.3±1.9 Mm^{-1}), respectively. Across the sampling sites, abs_{365} correlated robustly (R^2= 0.73, p<0.05) with levoglucosan being a known tracer for biomass burning (BB); This implied that

https://doi.org/10.5194/egusphere-2025-6271
Preprint. Discussion started: 12 January 2026

BrC in the NCP was significantly affected by fresh emissions from BB, which aligns with the prior observations in China (Li et al., 2022b; Desyaterik et al., 2013; Li et al., 2023). Additionally, the BB emission was more pronounced in rural areas, as indicated by a higher mass fraction of levoglucosan to OM (0.67±0.39%), which was approximately 2.1 to 5 times higher than those in urban areas. These findings highlight the significant impact of anthropogenic combustion on air quality in the rural NCP. From Figure 2b, the average light-absorption of urban BrC in the NCP exhibited a decline of ~45% from 10.7±3.0 Mm^{-1} in 2018 to 5.8±2.2 Mm^{-1} in 2023. Beijing exhibited a more substantial reduction, where the abs_{365} was only 16% of that recorded a decade ago (Figure 2b). Even so, the averaged abs_{365} in the NCP still remains higher than that in Nanjing, Guangzhou and urban areas in developed counties (Table S2).

As a metric for characterizing the light absorptivity of BrC, the MAE at 365 nm (MAE_{365}) was quantified by the linear regression slope of abs_{365} against WSOC. As illustrated in Figure 2c, MAE_{365} exhibits a distinctly different spatial pattern relative to abs_{365}. A strikingly high MAE_{365} value was measured in JN (1.4±0.04 $m^2\ g^{-1}$), on par with those found in severely polluted regions like Xingtai, Xi'an and Delhi, India (1.2-1.6 $m^2\ g^{-1}$, in the cold season) (Li et al., 2023; Wu et al., 2020; Kirillova et al., 2014); And the MAE_{365} value also falls within the range for documented BrC emitted from residential coal combustion (e.g., 1.20-1.59 $m^2\ g^{-1}$ for bituminous coal) (Ni et al., 2021), suggesting that coal combustion is one of the potential sources of atmospheric BrC in JN. Additionally, TJ, LC and HD shared a comparable MAE_{365} value of approximately 1.1 $m^2\ g^{-1}$, which closely matchs the values associated with biomass burning-derived

https://doi.org/10.5194/egusphere-2025-6271
Preprint. Discussion started: 12 January 2026

BrC (1.2±0.3 m^2 g^{-1}) (Cao et al., 2021). This finding further indicated a significant effect of biomass burning on the wintertime BrC in the NCP, which can be corroborated by the CWT analysis. As shown in Figure 3, high CWT loadings for abs_{365} were predominantly associated with regions characterized by concentrated fire hotspots, especially in LC, HD and their adjacent areas. Of note, the MAE_{365} of the BrC in BJ was the lowest (0.71±0.02 m^2 g^{-1}), only half that of JN. This relatively weak light absorptivity of BrC in BJ may be attributable to substantial vehicle emissions, as BrC from this source typically exhibits relatively low MAE values, ranging from approximately 0.35 to 0.71 m^2 g^{-1} (Tang et al., 2020; Huang et al., 2022). Another possibility is that the aerosol in BJ was more aged as verified by a higher BeP/(BaP+BeP) ratio (Figure S5a). Previously, it has been confirmed both observationally and experimentally that BrC light-absorption would decay in the aerosol aging process (Hems et al., 2021; Qiu et al., 2024); A negative correlation between BeP/(BaP+BeP) and MAE_{365} further supported this hypothesis (Figure S5b). In Figure 2d, we can note that unlike the temporal evolution of abs_{365}, the MAE_{365} of the BrC at most sampling sites undergone indistinctive variations in response to the reduction in anthropogenic emission.

As depicted in Figure 4a, the optical properties of BrC in different periods are plotted in the AAE-MAE_{405} (log scale) space, with reference to the optically defined BrC classes proposed by Saleh (2020). On average, BrC across the sampling sites exhibits optical properties akin to those from biomass burning or coal combustion, falling into the "weakly" absorbing BrC class; This observation reinforced remarkable impacts of

https://doi.org/10.5194/egusphere-2025-6271
Preprint. Discussion started: 12 January 2026

combustion sources on BrC in the NCP. Of particular note, the BrC light-absorptivity was enhanced from clean ($PM_{2.5}$ < 75 μg m^{-3}) to haze ($PM_{2.5}$ >75 μg m^{-3}) periods at most sampling sites, coinciding with the increasing N:C ratio (Figure 4a). These findings indicated that N-containing compounds (NOCs) were the pivotal chromophores governing BrC optical properties in the NCP, as supported by a positive correlation between N:C ratio and abs_{365} (Figure 4b). Accordingly, a high N:C ratio was also associated with an elevated WSOC/OC ratio (Figure 4b), implying that the secondary formation was likely the predominant source of the N-containing chromophores in the NCP.

3.3 Secondary formation N-containing compounds in the NCP

To quantify the contribution of secondary formation to the water-soluble organic nitrogen, a tracer method analogous to that used for estimating secondary organic carbon (SOC) with EC as a tracer was adopted here (Text S2 in the Supplement). From the results illustrated in Figure 5a, a dominant role of secondary formation in WSON accumulation was observed across five sites. Specifically, secondary WSON (WSONsec) in BJ explained more than 64±21% of the total WSON, which was comparable to those at other urban sites but was approximately1.2-fold of that in LC. Such spatial pattern was attribute to the enhanced primary emission (e.g., biomass burning) in rural site. Additionally, the fractional contribution of WSONsec increased with the rising $PM_{2.5}$ levels (Figure S6) across sampling sites, particularly in BJ. Above findings further highlighted the critical role of secondary formation in regulating the abundance of strongly light-absorbing N-containing chromophores during haze periods.

https://doi.org/10.5194/egusphere-2025-6271
Preprint. Discussion started: 12 January 2026

3.3.1 Aerosol aqueous formation of light-absorbing NOCs

The secondary WSON formation can be affected by multiple factors, e.g., NH_4^+, NO_2, O_3, ALWC, pH and meteorological factors. To investigate the contributions of these factors to WSONsec, a random forest analysis was conducted here and demonstrated that atmospheric WSONsec in the NCP was largely affected by NH_4^+ (~48%) and ALWC (~28%), underscoring a critical role of ammonia-induced aqueous processing in driving WSONsec formation. This phenomenon is presumably prevalent across China, as it has been observed in the rural site (Xianghe) in the NCP, Yangtze River Delta, the Guanzhong Plain, and even the upper boundary layer (Liu et al., 2023; Wu et al., 2024a; Xiao et al., 2025). Previously, aqueous-phase reaction via α-dicarbonyls (e..g, methylglyoxal and glyoxal) with NH_3 have been identified as an important formation pathway for N-heterocyclic species (e.g., imidazoles, IMs) (Yang et al., 2024; Aiona et al., 2017; Lin et al., 2015), of which yield can be regulated by the chemical forms of ammonium in aerosol; Specially, the uptake coefficient of methylglyoxal/glyoxal (the prevalent α-dicarbonyls in the atmosphere) on $(NH_4)_2SO_4$ seed was significantly higher than on NH_4HSO_4 seed, thereby leading to an enhanced yield of N-heterocycles and their oligomers (Li et al., 2021b). Whereas it has been confirmed theoretically that the aerosol across five sites were characterized by abundant $(NH_4)_2SO_4$ and NH_4NO_3 as shown in Figure S7a and Text S3. These hygroscopic $(NH_4)_2SO_4$ particles would promote N-containing compounds formation via NH_3-mediated aqueous-phase chemistry. To further validate above assumption, IMs-related fragments (e.g., $C_3H_3N_2^+$ and $C_3H_4N_2^+$) were quantified by offline AMS analysis during

https://doi.org/10.5194/egusphere-2025-6271
Preprint. Discussion started: 12 January 2026

a humid haze episode across the NCP (Figure S2); During this event, the ALWC/(ALWC+$PM_{2.5}$) was approximately 1.5-fold of that observed in the remaining periods (Figure S7b), indicating that aerosols were far more likely to be in the liquid phase during this period. In the atmosphere, IMs can be either directly emitted from biomass burning or secondarily produced via aqueous reactions (Gao et al., 2021). As illustrated in Figure 5c and S8, IMs-related fragments weakly corrected with the levoglucosan+BkF (R^2=0.02, p>0.05) but strongly with ammonium (R^2=0.93, p<0.01), suggesting that a major fraction of the IMs-like heterocyclic compounds was secondarily formed during the humid event. Notably, as the haze episode evolved, the IMs/WSON (N:N) ratio increased dramatically across the NCP, reaffirming an important role of NH_3-induced chemistry in NOCs formation under moist environments.

Additionally, aerosol acidity also modulated the WSON formation, with relative importance being~8% (Figure 5b). Figure 5d clearly demonstrates a negative correlation between the mass fraction of WSONsec in the total WSON and aerosol pH, indicating that acidic condition likely favors NOCs formation. It is possible that ammonia would be more readily partitioned into acidic aerosol, thereby promoting the formation of ammonia-derived NOCs. Consistent with this hypothesis, our estimation of the gas-to-particle partitioning coefficient for NH_3 (ε_{NH3}) showed that ε_{NH3} at pH 3.0 was one order of magnitude higher than that at pH 5.0 (Text S3). And numerous experimental evidences have established that the reactions of NH_3/NH_4^+ with carbonyl are generally acid catalyzed (Liu et al., 2015b; Zhang et al., 2015); Furthermore, our recent findings confirmed that compared to the neutral aerosols, acidic aerosols are

https://doi.org/10.5194/egusphere-2025-6271
Preprint. Discussion started: 12 January 2026

more conducive to the formation of high-molecular-weight NOCs though carbonyl-to-NH_3 reactions, which exhibit stronger light-absorptivity (Zhang et al., 2024).

3.3.2 Gas-phase formation of light-absorbing NOCs

It is worth noting that NO_2 and O_3 explained over 8% and 6% of the variances in the WSONsec (Figure 5b), implying that partial WSONsec presumably formed by gas-phase photochemical oxidation under relatively high NOx loadings. To verify this, nine NACs herein were quantified, which typically derived from gas-phase reactions of polyphenols with OH/NO_3 radicals, and followed by partitioning into the aerosol. As shown in Figure 6a, 4-Nitrophenol (4NP) and 4-Nitrocatechol (4NC) were the dominant species among the detected NACs; On average, they accounted for 56.8%–74.0% and 10.3%–20.7% of the total NACs across the five sites, respectively. This finding is consistent with previous observations reported in Shanghai (Liu et al., 2023), Dezhou (Li et al., 2021a), and Xinglong (Sun et al., 2026).

Furthermore, secondary NACs was also quantified following the method of WSONsec. As depicted in Figure 6b, secondary formation played a dominant role in NACs accumulation, contributing approximately 46%–64% of total NACs across the five sites. The positive correlation between secondary NACs and NO_2 was indicative of gas-phase oxidation being a significant formation pathway for NACs during the campaign. Previously, it is well established that nitrite is an important source of aerosol aqueous-phase NO_2 radical (Vione et al., 2004), which can react with aromatic compounds (e.g., phenol or catechol) to yield corresponding NACs; However, secondary NACs ($NACs_{[sec]}$) were correlated weakly with NO_2^- and ALWC (Figure 6c),

https://doi.org/10.5194/egusphere-2025-6271
Preprint. Discussion started: 12 January 2026

suggesting a limited role of aqueous-phase reactions in $NACs_{[sec]}$ formation. Notably, the $NACs_{[sec]}$ exhibited a temperature-dependent pattern across all sampling sites (P<0.05, Figure 6c); It is possible that ambient temperature largely affected gas-to-particle partitioning of the NACs, thereby moderating the abundance of particulate NACs. On this basis, we theoretically estimated the fraction of particulate 4NP (Fp) relative to the total based on the Pankow's absorption equilibrium theory, obtaining an average Fp of 0.3±0.1 across the NCP; This predicted value was within the range of field observations (0.2 in Hongkong to 0.75 on Mt. Tai) (Li et al., 2022a; Chen et al., 2025). As depicted in Figure 6d, the Fp correlated positively with the particulate 4NP, again suggesting that partial NOCs are formed by gas-phase photooxidation reactions, subsequently partitioning into the aerosol.

4 Conclusion and implications

Synchronous observations of the optical properties and chemical compositions of atmospheric BrC were conducted at five sites across the NCP during the winter of 2023. The OM was identified as the predominant component of $PM_{2.5}$ at all sampling sites, accounting for 40%-55% of the $PM_{2.5}$. BrC in rural area exhibited a higher light-absorption, being approximately 1.1–3.5 folds of those recorded at urban sites. Compared with the previous observations, the average light absorption of urban BrC decreased substantially by roughly 45 over the period 2018–2023, which was mainly due to significant anthropogenic emission controls in the NCP. The average MAE_{365} ranged from 0.7±0.04 $m^2\ g^{-1}$ to 1.40±0.02 $m^2\ g^{-1}$, with a distinctly different spatial pattern. Specially, a strikingly high MAE_{365} value (1.40±0.02 $m^2\ g^{-1}$) was measured in

https://doi.org/10.5194/egusphere-2025-6271
Preprint. Discussion started: 12 January 2026

JN, falls within the range for BrC emitted from residential coal combustion; While, the MAE_{365} values of BrC (~1.1 m^2 g^{-1}) in TJ, LC and HD were closely matched the values associated with biomass burning-derived BrC. The MAE_{365} value in BJ was the lowest among all the sampling sites, which was likely ascribed to enhanced photobleaching during aerosol aging.

During the haze periods, we observe that the MAE_{365} of BrC at most sample sites was 1.5-fold of that in clean periods, indicating enhanced light-absorptivity of BrC the haze development. Of particular note, a parallel variation was also found for N:C ratio; These findings indicated that N-containing compounds (NOCs), as crucial chromophores governing BrC optical properties in the NCP, were abundantly formed in the aerosol aging process. Additionally, these secondary NOCs accounted for over 50% of the total on average, and were mainly formed though the ammonia-induced aerosol aqueous reaction. In the previous observation conducted on Mt. Hua (Wu et al., 2024a), we also revealed that ammonia-driven aerosol aqueous reactions can also significantly promote BrC formation during the air mass lifting process. Collectively, these findings demonstrate that ammonia-derived NOCs are likely prevalent in the boundary layer. Therefore, NH_3 is probably one of the key factors contributing to the high load of strongly light-absorbing BrC in China, of which emission control in China is indispensable for further alleviating haze and BrC pollution in the country.

https://doi.org/10.5194/egusphere-2025-6271
Preprint. Discussion started: 12 January 2026

Data availability. The primary data used in this study can be obtained from https://doi.org/10.5281/zenodo.17947347 (Wu, 2025). Other data utilized in the present study are available from the corresponding author on request.

Author contributions. G.W. designed research and contributed analytic tools. C.W., Z.L. B.X. and R.L. collected the samples. C.W. and Y.C. conducted the sample analysis. C.W. performed the data interpretation. C.W. and G.W. wrote the paper. All authors contributed to the paper with useful scientific discussions.

Competing interests. The authors declare no competing interest.

Acknowledgements. This work was financially supported by the National Natural Science Foundation of China (grant no. 42130704, 42477097) and the National Key Research and Development Program of China (grant no. 2023YFC3707401).

References

Aiona, P. K., Lee, H. J., Leslie, R., Lin, P., Laskin, A., Laskin, J., and Nizkorodov, S. A.: Photochemistry of Products of the Aqueous Reaction of Methylglyoxal with Ammonium Sulfate, Acs Earth and Space Chemistry, 1, 522-532, 10.1021/acsearthspacechem.7b00075, 2017.

Andreae, M. O. and Gelencsér, A.: Black carbon or brown carbon?: The nature of light-absorbing carbonaceous aerosols, Atmospheric Chemistry and Physics, 6, 3131-3148, 10.5194/acp-6-3131-2006, 2006.

Cao, T., Li, M. J., Zou, C. L., Fan, X. J., Song, J. Z., Jia, W. L., Yu, C. L., Yu, Z. Q., and Ping, P. A.: Chemical composition, optical properties, and oxidative potential of water- and methanol-soluble organic compounds emitted from the combustion of biomass materials and coal, Atmospheric Chemistry and Physics, 21, 13187-13205, 10.5194/acp-21-13187-2021, 2021.

Chen, H. B., Zhou, R. Z., Fang, L., Sun, H. L., Yang, Q. Y., Niu, H. Y., Liu, J. W., Tian, Y. Z., Cui, M., and Yan, C. Q.: Variations in optical properties of water- and methanol-soluble organic carbon in PM 2.5 in Tianjin and Handan over the Wintertime of 2018-2020, Atmospheric Research, 303, 10.1016/j.atmosres.2024.107332, 2024a.

Chen, J. M., Li, C. L., Ristovski, Z., Milic, A., Gu, Y. T., Islam, M. S., Wang, S. X., Hao, J. M., Zhang, H. F., He, C. R., Guo, H., Fu, H. B., Miljevic, B., Morawska,

https://doi.org/10.5194/egusphere-2025-6271
Preprint. Discussion started: 12 January 2026

L., Thai, P., Lam, Y. F., Pereira, G., Ding, A. J., Huang, X., and Dumka, U. C.: A review of biomass burning: Emissions and impacts on air quality, health and climate in China, Science of the Total Environment, 579, 1000-1034, 10.1016/j.scitotenv.2016.11.025, 2017.

Chen, Q., Miao, R. Q., Geng, G. N., Shrivastava, M., Dao, X., Xu, B. Y., Sun, J. Q., Zhang, X., Liu, M. Y., Tang, G. G., Tang, Q., Hu, H. W., Huang, R. J., Wang, H., Zheng, Y., Qin, Y., Guo, S., Hu, M., and Zhu, T.: Widespread 2013-2020 decreases and reduction challenges of organic aerosol in China, Nature Communications, 15, 10.1038/s41467-024-48902-0, 2024b.

Chen, Y., Xia, M., Zheng, P. G., Li, Y. M., Zou, Z. X., Tong, S. R., Li, K., Feng, X., Hui, L. R., Yuan, Q., Li, J. J., Yu, J. Z., Lee, S. C., Wang, T., and Wang, Z.: Complex gas-particle partitioning of nitro-phenolic compounds: field-based insights and determination of apparent activity coefficient, Npj Climate and Atmospheric Science, 8, 10.1038/s41612-025-01156-z, 2025.

Daellenbach, K. R., Uzu, G., Jiang, J. H., Cassagnes, L. E., Leni, Z., Vlachou, A., Stefenelli, G., Canonaco, F., Weber, S., Segers, A., Kuenen, J. J. P., Schaap, M., Favez, O., Albinet, A., Aksoyoglu, S., Dommen, J., Baltensperger, U., Geiser, M., El Haddad, I., Jaffrezo, J. L., and Prévôt, A. S. H.: Sources of particulate-matter air pollution and its oxidative potential in Europe, Nature, 587, 414-+, 10.1038/s41586-020-2902-8, 2020.

Desyaterik, Y., Sun, Y., Shen, X. H., Lee, T. Y., Wang, X. F., Wang, T., and Collett, J. L.: Speciation of "brown" carbon in cloud water impacted by agricultural biomass burning in eastern China, Journal of Geophysical Research-Atmospheres, 118, 7389-7399, 10.1002/jgrd.50561, 2013.

Fang, T., Lakey, P. S. J., Weber, R. J., and Shiraiwa, M.: Oxidative Potential of Particulate Matter and Generation of Reactive Oxygen Species in Epithelial Lining Fluid, Environmental Science & Technology, 53, 12784-12792, 10.1021/acs.est.9b03823, 2019.

Feng, Y., Ramanathan, V., and Kotamarthi, V. R.: Brown carbon: a significant atmospheric absorber of solar radiation?, Atmospheric Chemistry and Physics, 13, 8607-8621, 10.5194/acp-13-8607-2013, 2013.

Finewax, Z., de Gouw, J. A., and Ziemann, P. J.: Identification and Quantification of 4-Nitrocatechol Formed from OH and NO3 Radical-Initiated Reactions of Catechol in Air in the Presence of NOx: Implications for Secondary Organic Aerosol Formation from Biomass Burning, Environmental Science & Technology, 52, 1981-1989, 10.1021/acs.est.7b05864, 2018.

Fu, X., Wang, S. X., Xing, J., Zhang, X. Y., Wang, T., and Hao, J. M.: Increasing Ammonia Concentrations Reduce the Effectiveness of Particle Pollution Control Achieved via SO2 and NOX Emissions Reduction in East China, Environmental Science & Technology Letters, 4, 221-227, 10.1021/acs.estlett.7b00143, 2017.

Gao, K., Zhang, Y. D., Liu, Y. Y., Yang, M. G., and Zhu, T.: Screening of imidazoles in atmospheric aerosol particles using a hybrid targeted and untargeted method based on ultra-performance liquid chromatography-quadrupole time-of-flight mass spectrometry, Analytica Chimica Acta, 1163, 10.1016/j.aca.2021.338516, 2021.

https://doi.org/10.5194/egusphere-2025-6271
Preprint. Discussion started: 12 January 2026

Ge, X. L., Sun, Y. L., Trousdell, J., Chen, M. D., and Zhang, Q.: Enhancing characterization of organic nitrogen components in aerosols and droplets using high-resolution aerosol mass spectrometry, Atmospheric Measurement Techniques, 17, 423-439, 10.5194/amt-17-423-2024, 2024.

Gligorovski, S., Strekowski, R., Barbati, S., and Vione, D.: Environmental Implications of Hydroxyl Radicals (•OH), Chemical Reviews, 115, 13051-13092, 10.1021/cr500310b, 2015.

Gong, Y. Q., Huang, R. J., Yang, L., Wang, T., Yuan, W., Xu, W., Cao, W. J., Wang, Y., and Li, Y. J.: Measurement report: Brown carbon aerosol in polluted urban air of the North China Plain - day-night differences in the chromophores and optical properties, Atmospheric Chemistry and Physics, 23, 15197-15207, 10.5194/acp-23-15197-2023, 2023.

Grace, D. N., Lugos, E. N., Ma, S. Q., Griffith, D. R., Hendrickson, H. P., Woo, J. L., and Galloway, M. M.: Brown Carbon Formation Potential of the Biacetyl-Ammonium Sulfate Reaction System, Acs Earth and Space Chemistry, 4, 1104-1113, 10.1021/acsearthspacechem.0c00096, 2020.

Hammer, M. S., Martin, R. V., van Donkelaar, A., Buchard, V., Torres, O., Ridley, D. A., and Spurr, R. J. D.: Interpreting the ultraviolet aerosol index observed with the OMI satellite instrument to understand absorption by organic aerosols: implications for atmospheric oxidation and direct radiative effects, Atmospheric Chemistry and Physics, 16, 2507-2523, 10.5194/acp-16-2507-2016, 2016.

He, S. and Carmichael, G. R.: Sensitivity of photolysis rates and ozone production in the troposphere to aerosol properties, Journal of Geophysical Research-Atmospheres, 104, 26307-26324, 10.1029/1999jd900789, 1999.

Hems, R. F. and Abbatt, J. P. D.: Aqueous Phase Photo-oxidation of Brown Carbon Nitrophenols: Reaction Kinetics, Mechanism, and Evolution of Light Absorption, Acs Earth and Space Chemistry, 2, 225-234, 10.1021/acsearthspacechem.7b00123, 2018.

Hems, R. F., Schnitzler, E. G., Liu-Kang, C., Cappa, C. D., and Abbatt, J. P. D.: Aging of Atmospheric Brown Carbon Aerosol, Acs Earth and Space Chemistry, 5, 722-748, 10.1021/acsearthspacechem.0c00346, 2021.

Hu, X. F., Belle, J. H., Meng, X., Wildani, A., Waller, L. A., Strickland, M. J., and Liu, Y.: Estimating PM2.5 Concentrations in the Conterminous United States Using the Random Forest Approach, Environmental Science & Technology, 51, 6936-6944, 10.1021/acs.est.7b01210, 2017.

Huang, R. J., Yuan, W., Yang, L., Yang, H. N., Cao, W. J., Guo, J., Zhang, N. N., Zhu, C. S., Wu, Y. F., and Zhang, R. J.: Concentration, optical characteristics, and emission factors of brown carbon emitted by on-road vehicles, Science of the Total Environment, 810, 10.1016/j.scitotenv.2021.151307, 2022.

Jiang, H. H., Frie, A. L., Lavi, A., Chen, J. Y., Zhang, H. F., Bahreini, R., and Lin, Y. H.: Brown Carbon Formation from Nighttime Chemistry of Unsaturated Heterocyclic Volatile Organic Compounds, Environmental Science & Technology Letters, 6, 184-190, 10.1021/acs.estlett.9b00017, 2019.

Jiang, X. T., Liu, D. T., Li, Q., Tian, P., Wu, Y. Z., Li, S. Y., Hu, K., Ding, S., Bi, K., Li,

https://doi.org/10.5194/egusphere-2025-6271
Preprint. Discussion started: 12 January 2026

R. J., Huang, M. Y., Ding, D. P., Chen, Q. C., Kong, S. F., Li, W. J., Pang, Y., and He, D.: Connecting the Light Absorption of Atmospheric Organic Aerosols with Oxidation State and Polarity, Environmental Science & Technology, 10.1021/acs.est.2c02202, 2022.

Jo, D. S., Park, R. J., Lee, S., Kim, S. W., and Zhang, X. L.: A global simulation of brown carbon: implications for photochemistry and direct radiative effect, Atmospheric Chemistry and Physics, 16, 3413-3432, 10.5194/acp-16-3413-2016, 2016.

Kirillova, E. N., Andersson, A., Tiwari, S., Srivastava, A. K., Bisht, D. S., and Gustafsson, Ö.: Water-soluble organic carbon aerosols during a full New Delhi winter: Isotope-based source apportionment and optical properties, Journal of Geophysical Research-Atmospheres, 119, 3476-3485, 10.1002/2013jd020041, 2014.

Lack, D. A., Langridge, J. M., Bahreini, R., Cappa, C. D., Middlebrook, A. M., and Schwarz, J. P.: Brown carbon and internal mixing in biomass burning particles, Proceedings of the National Academy of Sciences of the United States of America, 109, 14802-14807, 10.1073/pnas.1206575109, 2012.

Laskin, A., Laskin, J., and Nizkorodov, S. A.: Chemistry of Atmospheric Brown Carbon, Chemical Reviews, 115, 4335-4382, 10.1021/cr5006167, 2015.

Li, D. P., Wu, C., Zhang, S., Lei, Y. L., Lv, S. J., Du, W., Liu, S. J., Zhang, F., Liu, X. D., Liu, L., Meng, J. J., Wang, Y. S., Gao, J., and Wang, G. H.: Significant coal combustion contribution to water-soluble brown carbon during winter in Xingtai, China: Optical properties and sources, Journal of Environmental Sciences, 124, 892-900, 10.1016/j.jes.2022.02.026, 2023.

Li, K., Jacob, D. J., Liao, H., Shen, L., Zhang, Q., and Bates, K. H.: Anthropogenic drivers of 2013-2017 trends in summer surface ozone in China, Proceedings of the National Academy of Sciences of the United States of America, 116, 422-427, 10.1073/pnas.1812168116, 2019.

Li, M., Wang, X. F., Zhao, Y. N., Du, P., Li, H. Y., Li, J. R., Shen, H. Q., Liu, Z. Y., Jiang, Y. R., Chen, J., Bi, Y. J., Zhao, Y., Xue, L. K., Wang, Y., Chen, J. M., and Wang, W. X.: Atmospheric Nitrated Phenolic Compounds in Particle, Gaseous, and Aqueous Phases During Cloud Events at a Mountain Site in North China: Distribution Characteristics and Aqueous-Phase Formation, Journal of Geophysical Research-Atmospheres, 127, 10.1029/2022jd037130, 2022a.

Li, X., Hu, M., Wang, Y. J., Xu, N., Fan, H. Y., Zong, T. M., Wu, Z. J., Guo, S., Zhu, W. F., Chen, S. Y., Dong, H. B., Zeng, L. M., Yu, X. N., and Tang, X. Y.: Links between the optical properties and chemical compositions of brown carbon chromophores in different environments: Contributions and formation of functionalized aromatic compounds, Science of the Total Environment, 786, 10.1016/j.scitotenv.2021.147418, 2021a.

Li, X. R., Sun, N. N., Jin, Q. H., Zhao, Z. Y., Wang, L. L., Wang, Q. L., Gu, X., Li, Y. X., and Liu, X. A.: Light absorption properties of black and brown carbon in winter over the North China Plain: Impacts of regional biomass burning, Atmospheric Environment, 278, 10.1016/j.atmosenv.2022.119100, 2022b.

https://doi.org/10.5194/egusphere-2025-6271
Preprint. Discussion started: 12 January 2026

Li, Y., Ji, Y., Zhao, J., Wang, Y., Shi, Q., Peng, J., Wang, Y., Wang, C., Zhang, F., Wang, Y., Seinfeld, J. H., and Zhang, R.: Unexpected Oligomerization of Small α-Dicarbonyls for Secondary Organic Aerosol and Brown Carbon Formation, Environmental Science & Technology, 55, 4430-4439, 10.1021/acs.est.0c08066, 2021b.

Li, Y. M., Fu, T. M., Yu, J. Z., Zhang, A. X., Yu, X., Ye, J. H., Zhu, L., Shen, H. Z., Wang, C., Yang, X., Tao, S., Chen, Q., Li, Y., Li, L., Che, H. Z., and Heald, C. L.: Nitrogen dominates global atmospheric organic aerosol absorption, Science, 387, 10.1126/science.adr4473, 2025.

Lin, P., Laskin, J., Nizkorodov, S. A., and Laskin, A.: Revealing Brown Carbon Chromophores Produced in Reactions of Methylglyoxal with Ammonium Sulfate, Environmental Science & Technology, 49, 14257-14266, 10.1021/acs.est.5b03608, 2015.

Liu, D. T., He, C. L., Schwarz, J. P., and Wang, X.: Lifecycle of light-absorbing carbonaceous aerosols in the atmosphere, Npj Climate and Atmospheric Science, 3, 10.1038/s41612-020-00145-8, 2020.

Liu, J., Scheuer, E., Dibb, J., Diskin, G. S., Ziemba, L. D., Thornhill, K. L., Anderson, B. E., Wisthaler, A., Mikoviny, T., Devi, J. J., Bergin, M., Perring, A. E., Markovic, M. Z., Schwarz, J. P., Campuzano-Jost, P., Day, D. A., Jimenez, J. L., and Weber, R. J.: Brown carbon aerosol in the North American continental troposphere: sources, abundance, and radiative forcing, Atmospheric Chemistry and Physics, 15, 7841-7858, 10.5194/acp-15-7841-2015, 2015a.

Liu, X. D., Wang, H. Y., Wang, F. L., Lv, S. J., Wu, C., Zhao, Y., Zhang, S., Liu, S. J., Xu, X. B., Lei, Y. L., and Wang, G. H.: Secondary Formation of Atmospheric Brown Carbon in China Haze: Implication for an Enhancing Role of Ammonia, Environmental Science & Technology, 57, 11163-11172, 10.1021/acs.est.3c03948, 2023.

Liu, Y., Liggio, J., Staebler, R., and Li, S. M.: Reactive uptake of ammonia to secondary organic aerosols: kinetics of organonitrogen formation, Atmospheric Chemistry and Physics, 15, 13569-13584, 10.5194/acp-15-13569-2015, 2015b.

Ni, H. Y., Huang, R. J., Pieber, S. M., Corbin, J. C., Stefenelli, G., Pospisilova, V., Klein, F., Gysel-Beer, M., Yang, L., Baltensperger, U., El Haddad, I., Slowik, J. G., Cao, J. J., Prévôt, A. S. H., and Dusek, U.: Brown Carbon in Primary and Aged Coal Combustion Emission, Environmental Science & Technology, 55, 5701-5710, 10.1021/acs.est.0c08084, 2021.

Pankow, J. F., Seinfeld, J. H., Asher, W. E., and Erdakos, G. B.: Modeling the formation of secondary organic aerosol.: 1.: Application of theoretical principles to measurements obtained in the α-pinene/, β- pinene/, sabinene/, Δ3-carene/, and cyclohexene/ozone systems, Environmental Science & Technology, 35, 1164-1172, 10.1021/es001321d, 2001.

Powelson, M. H., Espelien, B. M., Hawkins, L. N., Galloway, M. M., and De Haan, D. O.: Brown Carbon Formation by Aqueous-Phase Carbonyl Compound Reactions with Amines and Ammonium Sulfate, Environmental Science & Technology, 48, 985-993, 10.1021/es4038325, 2014.

https://doi.org/10.5194/egusphere-2025-6271
Preprint. Discussion started: 12 January 2026

Qiu, Y. T., Qiu, T., Wu, Z. J., Liu, Y. N., Fang, W. X., Man, R. Q., Liu, Y. C., Wang, J. R., Meng, X. X. Y., Chen, J. C., Liang, D. P., Guo, S., and Hu, M.: Observational Evidence of Brown Carbon Photobleaching in Urban Atmosphere at Molecular Level, Environmental Science & Technology Letters, 11, 1032-1039, 10.1021/acs.estlett.4c00647, 2024.

Saleh, R.: From Measurements to Models: Toward Accurate Representation of Brown Carbon in Climate Calculations, Current Pollution Reports, 6, 90-104, 10.1007/s40726-020-00139-3, 2020.

Samset, B. H., Stjern, C. W., Andrews, E., Kahn, R. A., Myhre, G., Schulz, M., and Schuster, G. L.: Aerosol Absorption: Progress Towards Global and Regional Constraints, Current Climate Change Reports, 4, 65-83, 10.1007/s40641-018-0091-4, 2018.

Stockwell, C. E., Veres, P. R., Williams, J., and Yokelson, R. J.: Characterization of biomass burning emissions from cooking fires, peat, crop residue, and other fuels with high-resolution proton-transfer-reaction time-of-flight mass spectrometry, Atmospheric Chemistry and Physics, 15, 845-865, 10.5194/acp-15-845-2015, 2015.

Sun, Y., Sun, K., Wu, C., Zhang, H., Chen, Y., Li, Z., Li, R., Xiao, B., Ren, Y., and Wang, G.: Insights into the spatiotemporal differences of brown carbon in North China plain: Composition, optical properties and sources, Atmospheric Research, 331, 10.1016/j.atmosres.2025.108648, 2026.

Tang, J., Li, J., Su, T., Han, Y., Mo, Y. Z., Jiang, H. X., Cui, M., Jiang, B., Chen, Y. J., Tang, J. H., Song, J. Z., Peng, P. A., and Zhang, G.: Molecular compositions and optical properties of dissolved brown carbon in biomass burning, coal combustion, and vehicle emission aerosols illuminated by excitation-emission matrix spectroscopy and Fourier transform ion cyclotron resonance mass spectrometry analysis, Atmospheric Chemistry and Physics, 20, 2513-2532, 10.5194/acp-20-2513-2020, 2020.

Updyke, K. M., Nguyen, T. B., and Nizkorodov, S. A.: Formation of brown carbon via reactions of ammonia with secondary organic aerosols from biogenic and anthropogenic precursors, Atmospheric Environment, 63, 22-31, 10.1016/j.atmosenv.2012.09.012, 2012.

Vione, D., Maurino, V., Minero, C., Lucchiari, M., and Pelizzetti, E.: Nitration and hydroxylation of benzene in the presence of nitrite/nitrous acid in aqueous solution, Chemosphere, 56, 1049-1059, 10.1016/j.chemosphere.2004.05.027, 2004.

Vu, T. V., Shi, Z. B., Cheng, J., Zhang, Q., He, K. B., Wang, S. X., and Harrison, R. M.: Assessing the impact of clean air action on air quality trends in Beijing using a machine learning technique, Atmospheric Chemistry and Physics, 19, 11303-11314, 10.5194/acp-19-11303-2019, 2019.

Wang, D. W., Shen, Z. X., Bai, G. Z., Zhang, L. M., Huang, S. S., Zheng, H. H., Li, C. L., Sun, J., Xu, H. M., and Cao, J. J.: Oxidized Nitrogen-Containing Organic Compounds Formation Enhanced the Light Absorption of PM2.5 Brown Carbon, Journal of Geophysical Research-Atmospheres, 130, 10.1029/2024jd042960, 2025a.

https://doi.org/10.5194/egusphere-2025-6271
Preprint. Discussion started: 12 January 2026

Wang, G., Zhang, S., Wu, C., Zhu, T., Xu, X., Ge, S., Sun, H., Sun, Z., Wang, J., Ji, Y., Gao, J., Ren, Y., Li, H., Zhang, F., Wang, Y., and Seinfeld, J. H.: Atmospheric sulfate aerosol formation enhanced by interfacial anions, Pnas Nexus, 4, 10.1093/pnasnexus/pgaf058, 2025b.

Wang, G. H., Kawamura, K., Lee, S., Ho, K. F., and Cao, J. J.: Molecular, seasonal, and spatial distributions of organic aerosols from fourteen Chinese cities, Environmental Science & Technology, 40, 4619-4625, 10.1021/es060291x, 2006.

Wang, G. H., Zhang, R. Y., Gomez, M. E., Yang, L. X., Zamora, M. L., Hu, M., Lin, Y., Peng, J. F., Guo, S., Meng, J. J., Li, J. J., Cheng, C. L., Hu, T. F., Ren, Y. Q., Wang, Y. S., Gao, J., Cao, J. J., An, Z. S., Zhou, W. J., Li, G. H., Wang, J. Y., Tian, P. F., Marrero-Ortiz, W., Secrest, J., Du, Z. F., Zheng, J., Shang, D. J., Zeng, L. M., Shao, M., Wang, W. G., Huang, Y., Wang, Y., Zhu, Y. J., Li, Y. X., Hu, J. X., Pan, B., Cai, L., Cheng, Y. T., Ji, Y. M., Zhang, F., Rosenfeld, D., Liss, P. S., Duce, R. A., Kolb, C. E., and Molina, M. J.: Persistent sulfate formation from London Fog to Chinese haze, Proceedings of the National Academy of Sciences of the United States of America, 113, 13630-13635, 10.1073/pnas.1616540113, 2016.

Wang, L. Y., Zhang, L., Wang, G. H., An, X. Q., Wu, C., Chen, Y. B., Xie, Y. N., Lv, S. J., Wang, F. L., Li, L., Lu, Y. T., Che, H. Z., and Zhang, X. Y.: Notable Radiative Effects of Brown Carbon in China Haze, Geophysical Research Letters, 52, 10.1029/2025gl118037, 2025c.

Wang, Y. J., Hu, M., Wang, Y. C., Zheng, J., Shang, D. J., Yang, Y. D., Liu, Y., Li, X., Tang, R. Z., Zhu, W. F., Du, Z. F., Wu, Y. S., Guo, S., Wu, Z. J., Lou, S. R., Hallquist, M., and Yu, J. Z.: The formation of nitro-aromatic compounds under high NOx and anthropogenic VOC conditions in urban Beijing, China, Atmospheric Chemistry and Physics, 19, 7649-7665, 10.5194/acp-19-7649-2019, 2019.

Washenfelder, R. A., Attwood, A. R., Brock, C. A., Guo, H., Xu, L., Weber, R. J., Ng, N. L., Allen, H. M., Ayres, B. R., Baumann, K., Cohen, R. C., Draper, D. C., Duffey, K. C., Edgerton, E., Fry, J. L., Hu, W. W., Jimenez, J. L., Palm, B. B., Romer, P., Stone, E. A., Wooldridge, P. J., and Brown, S. S.: Biomass burning dominates brown carbon absorption in the rural southeastern United States, Geophysical Research Letters, 42, 653-664, 10.1002/2014gl062444, 2015.

Wong, J. P. S., Nenes, A., and Weber, R. J.: Changes in Light Absorptivity of Molecular Weight Separated Brown Carbon Due to Photolytic Aging, Environmental Science & Technology, 51, 8414-8421, 10.1021/acs.est.7b01739, 2017.

Wu, C., Chen, Y. B., Sun, Y. W., Zhang, H. J., Zhang, S., Cao, C., Li, J. J., and Wang, G. H.: Effects of anthropogenic pollutants on biogenic secondary organic aerosol formation in the atmosphere of Mt. Hua, China, Atmospheric Chemistry and Physics, 25, 11975-11989, 10.5194/acp-25-11975-2025, 2025.

Wu, C.: Simultaneous observation of brown carbon at five sites across the North China [data set], https://doi.org/10.5281/zenodo.17947347, 2025.

Wu, C., Liu, X., Zhang, K., Zhang, S., Cao, C., Li, J., Li, R., Zhang, F., and Wang, G.: Measurement report: Formation of tropospheric brown carbon in a lifting air mass, Atmospheric Chemistry and Physics, 24, 9263-9275, 10.5194/acp-24-9263-2024,

https://doi.org/10.5194/egusphere-2025-6271
Preprint. Discussion started: 12 January 2026

2024a.

Wu, C., Wang, G. H., Li, J., Li, J. J., Cao, C., Ge, S. S., Xie, Y. N., Chen, J. M., Li, X. R., Xue, G. Y., Wang, X. P., Zhao, Z. Y., and Cao, F.: The characteristics of atmospheric brown carbon in Xi'an, inland China: sources, size distributions and optical properties, Atmospheric Chemistry and Physics, 20, 2017-2030, 10.5194/acp-20-2017-2020, 2020.

Wu, Y. Z., Liu, Q., Liu, D. T., Tian, P., Xu, W. Q., Wang, J. F., Hu, K., Li, S. Y., Jiang, X. T., Wang, F., Huang, M. Y., Ding, D. P., Yu, C. J., and Hu, D. W.: Enhanced formation of nitrogenous organic aerosols and brown carbon after aging in the planetary boundary layer, Npj Climate and Atmospheric Science, 7, 10.1038/s41612-024-00726-x, 2024b.

Xiao, B., Wang, G., Li, Z., Li, R., Liang, C., Wang, H., Zhang, S., Wu, C., Li, R., Zhang, F., Zhang, R., Wu, Y., and Zhang, L.: High Contribution of Secondary Formation to Brown Carbon in China Humid Haze: Enhancing Role of Ammonia and Amines, Environmental Science & Technology, 10.1021/acs.est.5c13436, 2025.

Xie, M. J., Hays, M. D., and Holder, A. L.: Light-absorbing organic carbon from prescribed and laboratory biomass burning and gasoline vehicle emissions, Scientific Reports, 7, 10.1038/s41598-017-06981-8, 2017.

Yan, C. Q., Zheng, M., Bosch, C., Andersson, A., Desyaterik, Y., Sullivan, A. P., Collett, J. L., Zhao, B., Wang, S. X., He, K. B., and Gustafsson, Ö.: Important fossil source contribution to brown carbon in Beijing during winter, Scientific Reports, 7, 10.1038/srep43182, 2017.

Yang, L., Huang, R. J., Yuan, W., Huang, D. D., and Huang, C.: pH-Dependent Aqueous-Phase Brown Carbon Formation: Rate Constants and Implications for Solar Absorption and Atmospheric Photochemistry, Environmental Science & Technology, 58, 1236-1243, 10.1021/acs.est.3c07631, 2024.

Yang, Z. M., Tsona, N. T., George, C., and Du, L.: Nitrogen-Containing Compounds Enhance Light Absorption of Aromatic-Derived Brown Carbon, Environmental Science & Technology, 56, 4005-4016, 10.1021/acs.est.1c08794, 2022.

Zeng, L. H., Zhang, A. X., Wang, Y. H., Wagner, N. L., Katich, J. M., Schwarz, J. P., Schill, G. P., Brock, C., Froyd, K. D., Murphy, D. M., Williamson, C. J., Kupc, A., Scheuer, E., Dibb, J., and Weber, R. J.: Global Measurements of Brown Carbon and Estimated Direct Radiative Effects, Geophysical Research Letters, 47, 10.1029/2020gl088747, 2020.

Zhang, A. X., Wang, Y. H., Zhang, Y. Z., Weber, R. J., Song, Y. J., Ke, Z. M., and Zou, Y. F.: Modeling the global radiative effect of brown carbon: a potentially larger heating source in the tropical free troposphere than black carbon, Atmospheric Chemistry and Physics, 20, 1901-1920, 10.5194/acp-20-1901-2020, 2020.

Zhang, R. Y., Wang, G. H., Guo, S., Zarnora, M. L., Ying, Q., Lin, Y., Wang, W. G., Hu, M., and Wang, Y.: Formation of Urban Fine Particulate Matter, Chemical Reviews, 115, 3803-3855, 10.1021/acs.chemrev.5b00067, 2015.

Zhang, S., Gao, Y. N., Xu, X. B., Chen, L. Y., Wu, C., Li, Z., Li, R. J., Xiao, B. Y., Liu, X. D., Li, R., Zhang, F., and Wang, G. H.: Heterogeneous formation and light absorption of secondary organic aerosols from acetone photochemical reactions:

https://doi.org/10.5194/egusphere-2025-6271
Preprint. Discussion started: 12 January 2026

remarkably enhancing effects of seeds and ammonia, Atmospheric Chemistry and Physics, 24, 14177-14190, 10.5194/acp-24-14177-2024, 2024.

Zhang, Y. Z., Forrister, H., Liu, J. M., Dibb, J., Anderson, B., Schwarz, J. P., Perring, A. E., Jimenez, J. L., Campuzano-Jost, P., Wang, Y. H., Nenes, A., and Weber, R. J.: Top-of-atmosphere radiative forcing affected by brown carbon in the upper troposphere, Nature Geoscience, 10, 486-+, 10.1038/ngeo2960, 2017.

Zheng, B., Tong, D., Li, M., Liu, F., Hong, C., Geng, G., Li, H., Li, X., Peng, L., Qi, J., Yan, L., Zhang, Y., Zhao, H., Zheng, Y., He, K., and Zhang, Q.: Trends in China's anthropogenic emissions since 2010 as the consequence of clean air actions, Atmospheric Chemistry and Physics, 18, 14095-14111, 10.5194/acp-18-14095-2018, 2018.

Zuend, A. and Seinfeld, J. H.: Modeling the gas-particle partitioning of secondary organic aerosol: the importance of liquid-liquid phase separation, Atmospheric Chemistry and Physics, 12, 3857-3882, 10.5194/acp-12-3857-2012, 2012.

https://doi.org/10.5194/egusphere-2025-6271
Preprint. Discussion started: 12 January 2026

Table caption

Table 1 Optical properties of BrC, mass concentrations of chemical composition in $PM_{2.5}$, and meteorological parameters at sampling sites.

Figure captions

Figure 1 Chemical composition of $PM_{2.5}$ and sources for organic matters (OM) at different sampling sites. The mass concentration data correspond to $PM_{2.5}$. The maps are the reproductions from ©Mapbox (https://account.mapbox.com/, last access: 03 December 2025)

Figure 2 Optical properties of BrC at each sampling site. **(a** and **c)** Average absorption spectra and mass absorption coefficient of WSOC; **(b** and **d)** Comparison of abs_{365} and MAE_{365} in different cities of China (NJ, XA and GZ represent Nanjing, Xi'an and Guangzhou; Superscripts indicate the corresponding years, for instance, the superscript "11" refers to 2011; The datasets of (b) and (d) were derived from the literature, and given in Table S3).

Figure 3 The CWT analysis of BrC at sampling sites along with fire hotspot. Fire hotspot data from Fire Information for Resource Management System (FIRMS) were applied to evaluate open biomass burning intensity during the campaign. The data were acquired from the Visible Infrared Imaging Radiometer Suite (VIIRS) sensor and processed using a fire detection algorithm to identify active fire hotspots.

Figue 4 Graphical representation of optical-based BrC classes in $\log_{10}(MAE_{405})$-AAE space **(a)**. The shaded regions represent very weakly light-absorbing BrC (VW-BrC), weakly light-absorbing BrC (W-BrC), moderately light-absorbing BrC (M-BrC), strongly light-absorbing BrC (S-BrC), and absorbing BC, respectively. **(b)** shows the linear fit regressions for abs_{365} with N:C ratio.

Figure 5 Aqueous formation of N-containing compounds in the NCP. Fractional contribution of primary water-soluble organic nitrogen (WSONpri) and secondary WSON (WSONsec) to the total **(a)**; SHAP feature importance assessment for the key factors affecting WSONsec **(b)**; Linear correlation between IMs-related fragments and NH_4^+ with different $PM_{2.5}$ loads **(c)**; **(d)** show the linear fit regressions for WSONsec/WSON with pH value across the NCP.

Figure 6 Chemical composition and formation of NACs. Fractional mass contribution of individual NAC to the total (a); Relative contributions of primary emissions ($NACs_{[pri]}$) and secondary formation ($NACs_{[sec]}$) to the detected NACs (b); Linear

https://doi.org/10.5194/egusphere-2025-6271
Preprint. Discussion started: 12 January 2026

872 regression analysis for particulate 4NP with its gas-to-particle-phase partitioning
873 coefficient.
874
875
876 **Table 1** Optical properties of BrC, mass concentrations of chemical composition in
877 $PM_{2.5}$, and meteorological parameters at sampling sites.

	Beijing	Tianjin	Luancheng	Handan	Jinan
(i) Meteorological parameters and gaseous pollutants					
T (℃)	–1.1±5.6	–1.2±4.9	1.2±6.3	1.7±6.6	3.1±5.9
RH (%)	49±21	50±19	54±22	59±21	54±23
O_3 (μg m^{-3})	29±20	31±18	31±18	28±17	35±26
NO_2 (μg m^{-3})	41±26	48±31	44±23	46±18	48±60
SO_2 (μg m^{-3})	4±5	4.7±2.4	8.8±4.5	5.9±3.8	10.0±11.0
(ii) Mass concentrations of $PM_{2.5}$ and its chemical composition (μg m^{-3})					
$PM_{2.5}$	38±36	52±50	74±46	80±49	94±38
NO_3^-	5.4±7.3	13.0±14.6	19.0±18.2	22.7±20.8	17.3±13.4
SO_4^{2-}	1.8±1.0	4.6±4.0	6.7±7.0	7.0±5.8	7.5±5.8
NH_4^+	1.6±2.2	5.7±5.9	8.2±8.6	9.1±8.0	7.3±6.5
Cl^-	1.0±0.7	3.2±2.7	2.8±1.7	2.9±1.9	2.3±1.2
OM	9.1±5.2	7.9±5.7	18.5±11	18.7±10.7	16.3±7.3
EC	2.7±2.4	2.8±1.7	4.4±2.5	3.1±1.9	4.2±1.4
WSOC	3.2±1.8	4.9±3.1	7.3±4.0	7.5±4.1	4.8±1.7
WSON	0.65±0.64	1.2±1.1	2.5±2.6	2.3±1.6	1.3±0.8
(iii) Optical properties of BrC, ALWC and acidity of $PM_{2.5}$					
abs_{365} (Mm^{-3})	2.3±1.9	5.7±3.8	8.0±4.7	8.2±5.0	6.9±3.0
MAE (m^2 g^{-1})	0.71±0.5	1.12±0.05	1.10±0.04	1.05±0.02	1.4±0.02
pH	5.6±1.1	3.8±0.8	3.3±1.4	4.1±1.2	4.0±1.1
ALWC (μg m^{-3})	9.7±21.6	21.0±38	36±74	47±72	41±70

878 ALWC: aerosol liquid water content; ALWC and pH were simulated by thermodynamic model
879 (ISORROPIA-II), details can be found in Text S4.
880

https://doi.org/10.5194/egusphere-2025-6271
Preprint. Discussion started: 12 January 2026

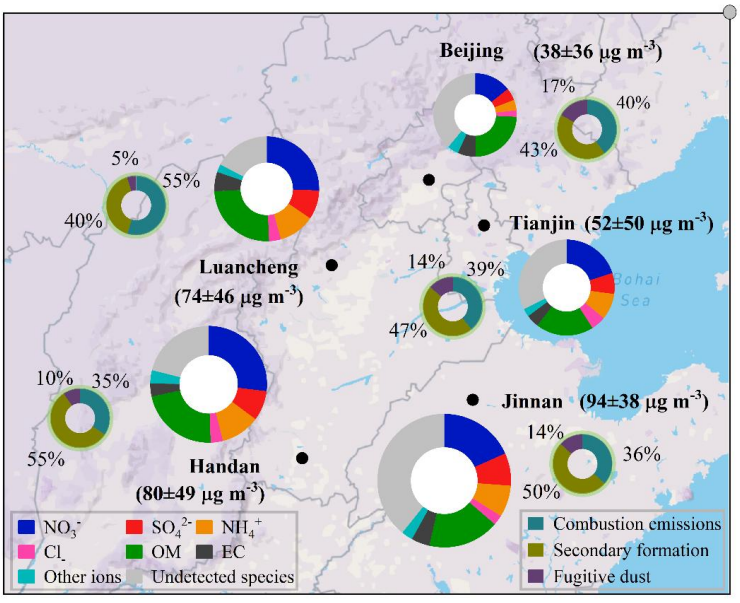

Figure 1 Chemical composition of $PM_{2.5}$ and sources for organic matters (OM) at different sampling sites. The mass concentration data correspond to $PM_{2.5}$. The maps are the reproductions from ©Mapbox (https://account.mapbox.com/, last access: 03 December 2025)

https://doi.org/10.5194/egusphere-2025-6271
Preprint. Discussion started: 12 January 2026

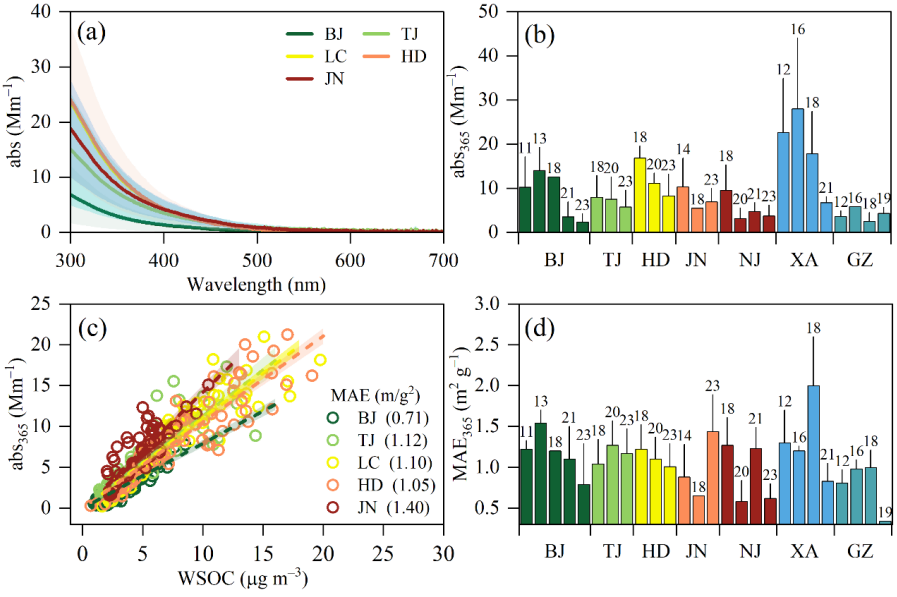

887

888 **Figure 2** Optical properties of BrC at each sampling site. **(a** and **c)** Average absorption
889 spectra and mass absorption coefficient of WSOC; **(b** and **d)** Comparison of abs_{365} and
890 MAE_{365} in different cities of China (NJ, XA and GZ represent Nanjing, Xi'an and
891 Guangzhou; Superscripts indicate the corresponding years, for instance, the superscript
892 "11" refers to 2011; The datasets of (b) and (d) were derived from the literature, and
893 given in Table S3).

894

895

https://doi.org/10.5194/egusphere-2025-6271
Preprint. Discussion started: 12 January 2026

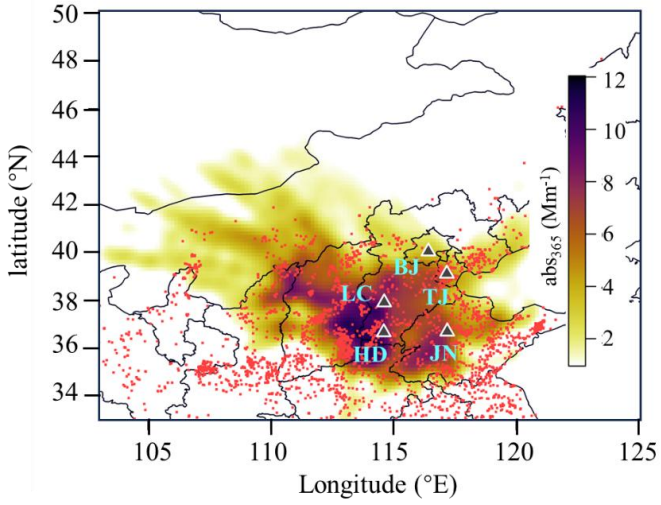

Figure 3 The CWT analysis of BrC at sampling sites along with fire hotspot. Fire hotspot data from Fire Information for Resource Management System (FIRMS) were applied to evaluate open biomass burning intensity during the campaign. The data were acquired from the Visible Infrared Imaging Radiometer Suite (VIIRS) sensor and processed using a fire detection algorithm to identify active fire hotspots.

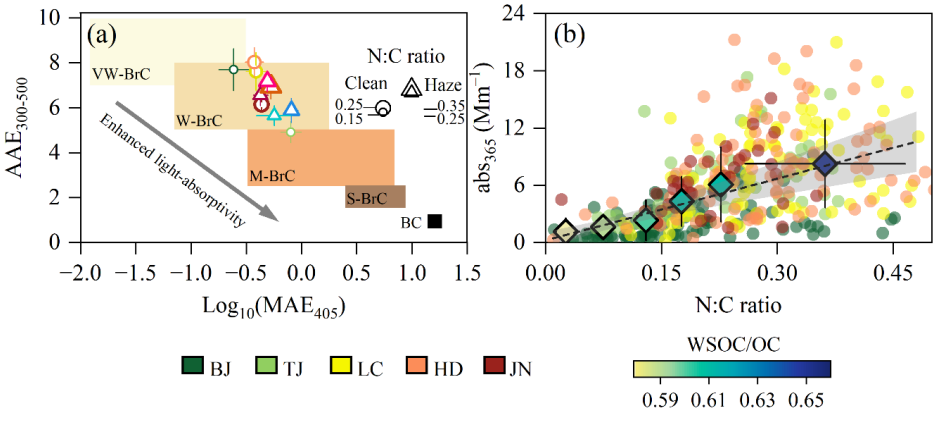

Figue 4 Graphical representation of optical-based BrC classes in $\log_{10}(MAE_{405})$-AAE space **(a)**. The shaded regions represent very weakly light-absorbing BrC (VW-BrC), weakly light-absorbing BrC (W-BrC), moderately light-absorbing BrC (M-BrC), strongly light-absorbing BrC (S-BrC), and absorbing BC, respectively. **(b)** shows the linear fit regressions for abs_{365} with N:C ratio.

https://doi.org/10.5194/egusphere-2025-6271
Preprint. Discussion started: 12 January 2026

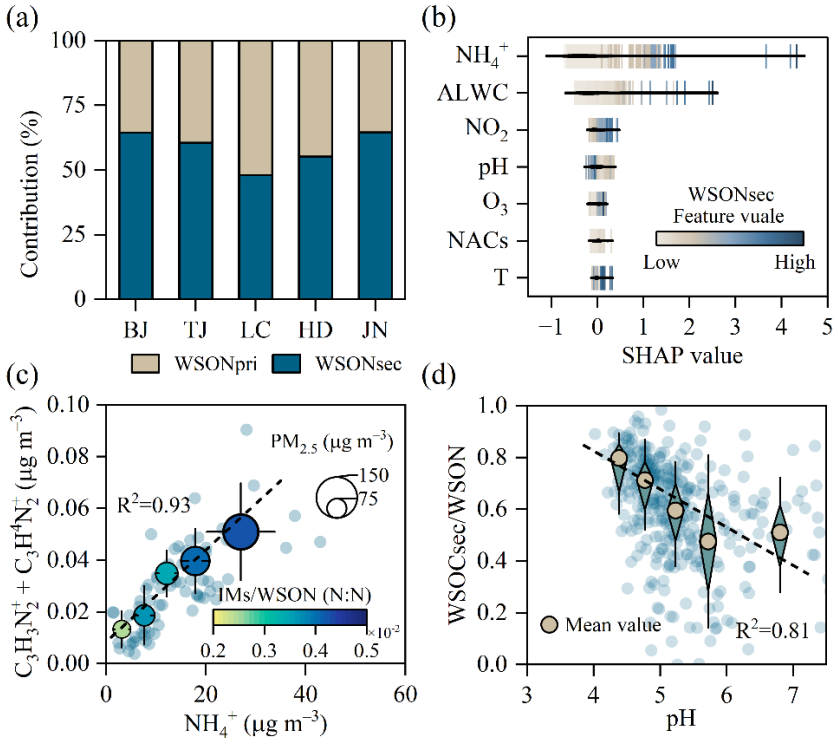

Figure 5 Aqueous formation of N-containing compounds in the NCP. Fractional contribution of primary water-soluble organic nitrogen (WSONpri) and secondary WSON (WSONsec) to the total **(a)**; SHAP feature importance assessment for the key factors affecting WSONsec **(b)**; Linear correlation between IMs-related fragments and NH_4^+ with different $PM_{2.5}$ loads **(c)**; **(d)** show the linear fit regressions for WSONsec/WSON with pH value across the NCP.

https://doi.org/10.5194/egusphere-2025-6271
Preprint. Discussion started: 12 January 2026

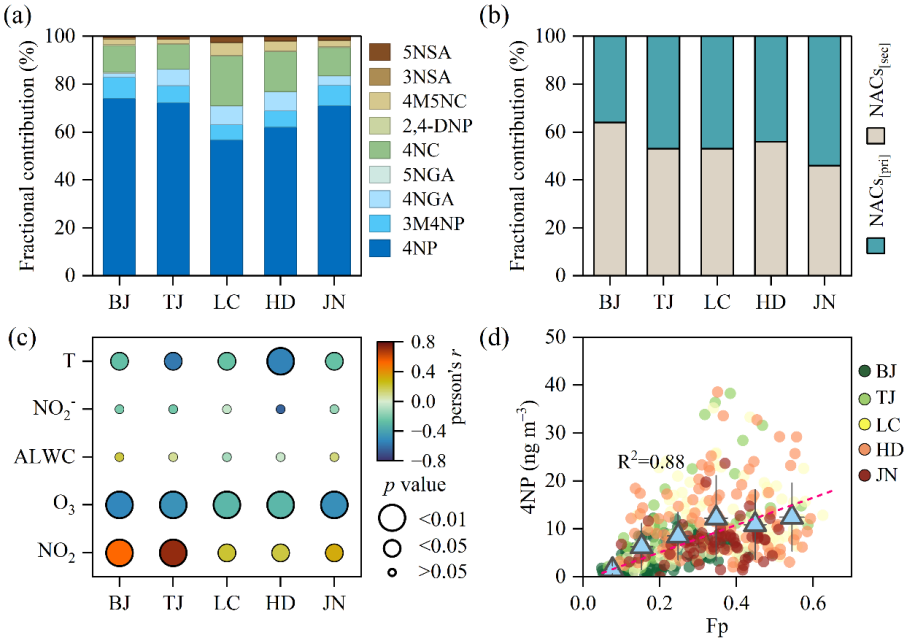

Figure 6 Chemical composition and formation of NACs. Fractional mass contribution of individual NAC to the total (a); Relative contributions of primary emissions ($NACs_{[pri]}$) and secondary formation ($NACs_{[sec]}$) to the detected NACs (b); Linear regression analysis for particulate 4NP with its gas-to-particle-phase partitioning coefficient.